Journal of Earth Science, *Vol. 32*, *No. 5*, *p. 1212–1225*, *October 2021* *ISSN 1674-487X*
Printed in China
https://doi.org/10.1007/s12583-020-1095-2

Decoupling between Oxygen and Radiogenic Isotopes: Evidence for Generation of Juvenile Continental Crust by Partial Melting of Subducted Oceanic Crust

Xuan-Ce Wang*[1, 2], Qiuli Li[3], Simon A. Wilde[1, 4], Zheng-Xiang Li[4], Chaofeng Li[3], Kai Lei[2], Shao-Jie Li[1], Linlin Li[1], Manoj K. Pandit[5]

1. *School of Earth Sciences*, *Yunnan University*, *Kunming* 650500, *China*
2. *School of Earth Science and Resources*, *Chang'an University*, *Xi'an* 710054, *China*
3. *State Key Laboratory of Lithospheric Evolution*, *Institute of Geology and Geophysics*, *Chinese Academy of Sciences*, *Beijing* 100029, *China*
4. *ARC Centre of Excellence for Core to Crust Fluid Systems and The Institute for Geoscience Research*, *Department of Applied Geology*, *Curtin University*, *Perth* 6845, *Australia*
5. *Department of Geology*, *University of Rajasthan*, *Jaipur* 302004, *India*

Xuan-Ce Wang: https://orcid.org/0000-0001-7276-6273

ABSTRACT: There is increasing evidence indicating that melts derived from subducted oceanic crust and sediments may have played a key role in building continental crust. This mechanism predicts that juvenile arc crust should have oxygen isotope characteristics ranging from mantle-like to supracrustal, but consistent mantle-like radiogenic (Nd-Hf) isotopic signatures. Here we present *in-situ* zircon U-Pb dating, Hf-O isotope analyses, and whole rock major-trace element and Nd isotope analyses of a granitoid from NW India. *In-situ* secondary ion mass spectrometry (SIMS) zircon U-Pb dating yields a weighted mean $^{207}Pb/^{206}Pb$ age of 873±6 Ma for the granitoid. It displays mantle-like zircon ε_{Hf} ($\varepsilon_{Hf(873\ Ma)}$= +9.3 to +10.9) and whole-rock Nd ($\varepsilon_{Nd(873\ Ma)}$= +3.5) values but supracrustal $\delta^{18}O$ values, the latter mostly varying between 9‰ and 10‰. The calculated whole-rock $\delta^{18}O$ value of 11.3‰±0.6‰ matches well with those of hydrothermally-altered pillow lavas and sheeted dykes from ophiolites. The major and trace element composition of the granitoid is similar to petrological experimental melts derived from a mixture of MORB+sediments. Thus, the granitoid most likely represents the product of partial melting of the uppermost oceanic crust (MORB+sediments). We propose that the decoupling between Hf-Nd and O isotopes as observed in this granitoid can be used as a powerful tool for the identification of slab melting contributing to juvenile continental crustal growth. Such isotopic decoupling can also account for high $\delta^{18}O$ values observed in ancient juvenile continental crust, such as Archean tonalite-trondhjemite-granodiorite suites.

KEY WORDS: zircon, Hf-Nd and O isotopes, decoupling, slab melting, Neoproterozoic continental crustal growth.

0 INTRODUCTION: PARTIAL MELTING OF BASALTIC ROCKS AS AN IMPORTANT MECHANISM FOR GENERATING JUVENILE CONTINENTAL CRUST

A paradox of Earth's juvenile continental crust is that, although its isotopic signatures imply the involvement of large volumes of new material with mantle-like isotopic signatures (e.g., Kemp et al., 2007), its major element composition indicates an insignificant input directly from the mantle (e.g., Hacker et al., 2011). For instance, the 425–390 Ma Lachlan I-type granitic rocks in southeastern Australia show a clear decoupling between Hf-O isotopes and major element compositions (Kemp et al., 2007). Zircon Hf-O isotopes indicate that the generation of the Lachlan I-type granitic melts involved 50 wt.% to 85 wt.% juvenile materials, whereas their major element compositions suggest that such a high proportion of juvenile materials could not have been derived directly from Earth's mantle (e.g., Chappell, 1996). Such a decoupling may therefore imply an indirect mantle input mechanism, through remelting of basaltic rocks shortly after their extraction from the mantle. Evidence from the Central Asian Orogenic Belt (CAOB; e.g., Kröner et al., 2007), the Greater Tibetan Plateau (Niu et al., 2013 and references therein), and modern oceanic arcs (Jagoutz and Schmidt, 2012) shows that the juvenile continental crust is characterized by mantle-like Sr-Nd isotopic ratios, but its major element composition is unlike basaltic mantle melts. The observed decoupling between radiogenic isotopes and major element compositions in juvenile continental crust requires a process whereby not only must it

*Corresponding author: x.wang4@uq.edu.au

Manuscript received April 27, 2020.
Manuscript accepted September 11, 2020.

Wang, X.-C., Li, Q. L., Wilde, S. A., et al., 2021. Decoupling between Oxygen and Radiogenic Isotopes: Evidence for Generation of Juvenile Continental Crust by Partial Melting of Subducted Oceanic Crust. *Journal of Earth Science*, 32(5): 1212–1225. https://doi.org/10.1007/s12583-020-1095-2. http://en.earth-science.net

preserve mantle-like radiogenic isotope signatures but also produce andesitic to felsic melts (Niu et al., 2013; Jagoutz and Schmidt, 2012). Partial melting of a mixture of mid-ocean ridge basalt (MORB)-derived amphibolite and biotite-rich metagreywacke at temperatures of 1 000–1 200 °C and pressures of 1.5–2.0 GPa can produce melts that strongly resemble andesitic arc crust (Castro et al., 2010). Thus, partial melting of mantle-derived basaltic rocks and metasediments shortly after their extraction from the mantle can account for the paradox of Earth's continental crustal composition (e.g., Castro et al., 2013, 2010; Niu et al., 2013).

Oceanic crust covers about sixty percent of Earth's surface and is a product of predominantly mantle melting (Klein, 2003). The resulting basaltic rocks are either recycled into the convecting mantle, or involved in building juvenile arc crust shortly after extraction from their mantle source (≤200 Ma; e.g., Castro et al., 2013, 2010; Niu et al., 2013; Spandler and Pirard, 2013; Jagoutz and Schmidt, 2012; Kelemen, 1995). This short residence time ensures that resultant melts can inherit the mantle-like radiogenic isotopic signatures of subducted oceanic crust. Experimental results have shown that melts of subducted oceanic basalts, plus minor terrestrial sediments at intermediate melt fractions, have chemical compositions similar to those of Archean TTGs and their Phanerozoic equivalents, the tonalite-trondhjemite-dacite suite (including adakites and Na-rich granitoids; Castro et al., 2010 and references therein). Thus, melting of subducted oceanic slabs may have played a key role in building arc crust (e.g., Behn et al., 2011).

The relationship between Hf and O isotopes is thus important for fingerprinting the contribution from slab melts in the growth of continental crust (see Wang et al., 2016 for a review). Oxygen isotopes are sensitive to surface water-rock interaction (e.g., Wang et al., 2011; Bindeman et al., 2005; Eiler, 2001; Eiler et al., 1998). With rare exceptions, the oxygen isotopic ratio of $^{18}O/^{16}O$ (usually expressed as the $\delta^{18}O$ value, reported relative to Vienna Standard Mean Ocean Water, VSMOW) is remarkably homogeneous in the mantle and in unaltered basaltic rocks, having a value of 5.3‰±0.3‰ and this has remained so throughout Earth's history (Valley et al., 1998; Mattey et al., 1994). In contrast, supracrustal materials or their recycled components have highly variable $\delta^{18}O$ values, commonly ranging between -10‰ and +30‰ (Bindeman et al., 2005; Valley et al., 2003; Eiler, 2001; Eiler et al., 1998). Low-temperature alteration produces high $\delta^{18}O$ values, whereas high-temperature alteration produces low $\delta^{18}O$ values (Bindeman et al., 2005; Eiler, 2001; Eiler et al., 1998). Hydrothermal alteration of the upper part of the oceanic lithosphere (pillow lavas, sheeted dykes, and gabbros) results in $\delta^{18}O$ values varying from about 2‰ to 16‰ (e.g., Yamaoka et al., 2012; Miller et al., 2001). Thus, juvenile continental crust derived from a mixture of subducted oceanic basalts and sediments is expected to possess mantle-like radiogenic (Hf and Nd), but supracrustal oxygen isotope signatures.

Identifying the reasons for the decoupling between mantle-like Hf and supracrustal oxygen isotopes in juvenile continental crustal rocks is crucial for understanding how they were generated. Granitic rocks have played a key role in building continental crust and are ideal for testing the predicted decoupling signatures. In this work, we conducted whole-rock major and trace elements, Nd isotope, and *in-situ* zircon U-Pb dating and Hf-O isotope analyses on a Neoproterozoic granitoid from NW India (Fig. 1a). The sample has a mantle-like whole-rock Nd and zircon Hf isotopic composition, but a supracrustal zircon O isotopic signature. Our work demonstrates that decoupling between mantle-like radiogenic and supracrustal oxygen isotopes can be used as a diagnostic feature for the presence of slab (oceanic basalts+sediments) melts in juvenile continental crust.

1 GEOLOGICAL BACKGROUND AND SAMPLE LOCATION

The granitoid sample (RJ06) was collected from the northwestern Indian Block, near Sindreth/Sirohi (Fig. 1). The NW Indian Block consists of an Archean basement (the 3.3–2.5 Ga Banded Gneiss Complex, Pandit et al., 2003 and references therein) and two Proterozoic supracrustal sequences, the Aravalli (Paleoproterozoic) and Delhi (Mesoproterozoic) supergroups, which uncomfortably overlie the basement. The Aravalli-Delhi fold belt (ADFB) can be traced over more than 750 km as a NE-trending linear orogenic belt (Fig. 1a). The ADFB underwent multiple deformation and metamorphism up to amphibolite facies. The western margin of the ADFB is marked by a suture along which the western Marwar terrane collided with the Aravalli craton at ca. 1.0 Ga (Deb et al., 2001). The suture zone is defined by the Phulad ophiolite zone (Volpe and Macdougall, 1990; Fig. 1a). The collision caused juxtaposition of arc remnants (Sendra-Ambaji arc terrane; Fig. 1a) and metasediments of the Delhi Basin (quartzites and calcsilicates) with granulite facies terranes (the Mangalwar and Sand Mata terranes; Fig. 1a) in the southern segment of the ADFB by east-verging thrusting and stacking (Pandit et al., 2003; Deb et al., 2001). The 968±1 Ma calc-alkaline Sendra granitoids (Pandit et al., 2003) and 990±6 and 987±6 Ma rhyolites (Deb et al., 2001) constrain the age of the Sendra-Ambaji arc terrane (Fig. 1a). Crustal convergence also initiated ophiolite obduction (the Phulad Ophiolite; Fig. 1a) onto the arc. This continental collision is also recorded by 0.97−0.90 Ga metamorphic events in the high-pressure granulite facies Mangalwar and Sandmata terranes (Buick et al., 2010 and references therein).

The late stage of the orogenic event is defined by several granitic intrusions parallel to the trend of the ADFB and in the region further to the west. These intrusions, loosely termed the Erinpura granites, are variably deformed, with texture varying in outcrop from phaneritic granite to gneiss and have been proposed to represent a syn- to late orogenic phase of magmatism formed during the Delhi orogeny (Just et al., 2011; Pandit et al., 2003; Deb et al., 2001; Naik, 1993; Choudhary et al., 1984). Subduction/orogeny may be related to the global Grenvillian event resulting in amalgamation of crustal blocks to form the supercontinent Rodinia.

These granitoids, as noted above, are conventionally regarded as manifestations of late thermal events related to the 1 Ga Delhi orogeny, although available age data on the Erinpura granites are scarce. Conventionally, the whole-rock Rb-Sr date of 830 Ma for granites at Erinpura and 820 Ma for granitoid at Pali (Fig. 1b), as well as the U-Pb TIMS ages, including 836+7/-5 Ma for the Siyawa granite and 800±2 Ma for the Pali granite (Just et al., 2011; van Lente et al., 2009 and references therein), have been considered to define the age of the granitoid. Van Lente et

al. (2009) also reported a discordant U-Pb zircon TIMS age of 873±3 Ma for a small tonalite body from the Pali area (Fig. 1b). Recent studies of monazites from the Erinpura granitoids indicate protolith crystallization at 863±23 Ma and recrystallization and formation of new Th-poor monazite at 775±26 Ma during shearing (Just et al., 2011). Solanki (2011) obtained a ca. 870 Ma zircon U-Pb age on granitic gneiss from the Erinpura granite and 848.1±7.1 Ma on the Ranakpur quartz syenite. All available data suggest that these rocks were generated during the assembly of the Rodinia supercontinent (Pandit et al., 2003). However, the inter-relationship between these magmatic events is currently unclear and the tectono-thermal history of the Erinpura granites is still poorly constrained.

The most extensive thermal event in the region surrounding the Erinpura granites resulted in the formation of the 770–750 Ma Malani igneous suite (MIS; Fig. 1a) (Ashwal et al., 2013 and references therein), predominantly composed of felsic rocks that occur as isolated outcrops extending over more than 50 000 km^2. The Malani rocks are undeformed and unmetamorphosed (generally A-type or I-type granites) and are quite distinct from the predominantly S-type characteristics and variably-deformed and metamorphosed nature of the Erinpura granites (Ashwal et al., 2013). Some exposures of crudely-foliated granodiorite and granitic gneiss are present in a small area around Harsani, along the western margin of the MIS (Fig. 1b). These are clearly distinct from the MIS rocks in terms of mineralogy and deformation/metamorphic history and were initially referred to as 'unclassified granites'. Pandit et al. (1999) conducted the first detailed study on them and described them as pre-Malani granitoids, consisting of an older trondhjemitic gneiss and a younger granodiorite. The granodiorite was dated at 827±9 Ma (zircon U-Pb, Pradhan et al., 2010) and is therefore coeval with some of the Erinpura granites. In this study, we sampled the older trondhjemitic gneiss from near Sindreth/Sirohi (sample RJ06; Fig. 1b). It occurs as an exposure within interdunal depressions and shows well-defined NNE to NW trending foliations. Petrographic examination has identified Na-plagioclase (sericitized oligoclase) and K-feldspar, with flattened quartz grains and biotite defining the foliation. Minor microcline occupies interstitial spaces, whereas zircon, titanite and apatite occur as accessory phases. These rocks were described as metaluminous I-type granite by Pandit et al. (1999).

2 SAMPLE PREPARATION AND ANALYTICAL TECHNIQUES

2.1 Whole-Rock Geochemistry

Sample RJ06 was sawn into slabs and the fresh central parts (>200 g) were used for bulk-rock geochemical analysis. The sample was crushed into small fragments (<0.5 cm in diameter) and powdered in a corundum mill. Bulk-rock major element analyses were carried out at the Guangzhou Institute of Geochemistry, Chinese Academy of Sciences. Whole-rock major element oxides were analyzed using a RigakuRIX 2000 X-ray fluorescence spectrometer (XRF) with determined uncertainties of <3% for SiO_2, Al_2O_3, Fe_2O_3, MgO, CaO, Na_2O, and K_2O, and <5% for TiO_2, MnO, and P_2O_5.

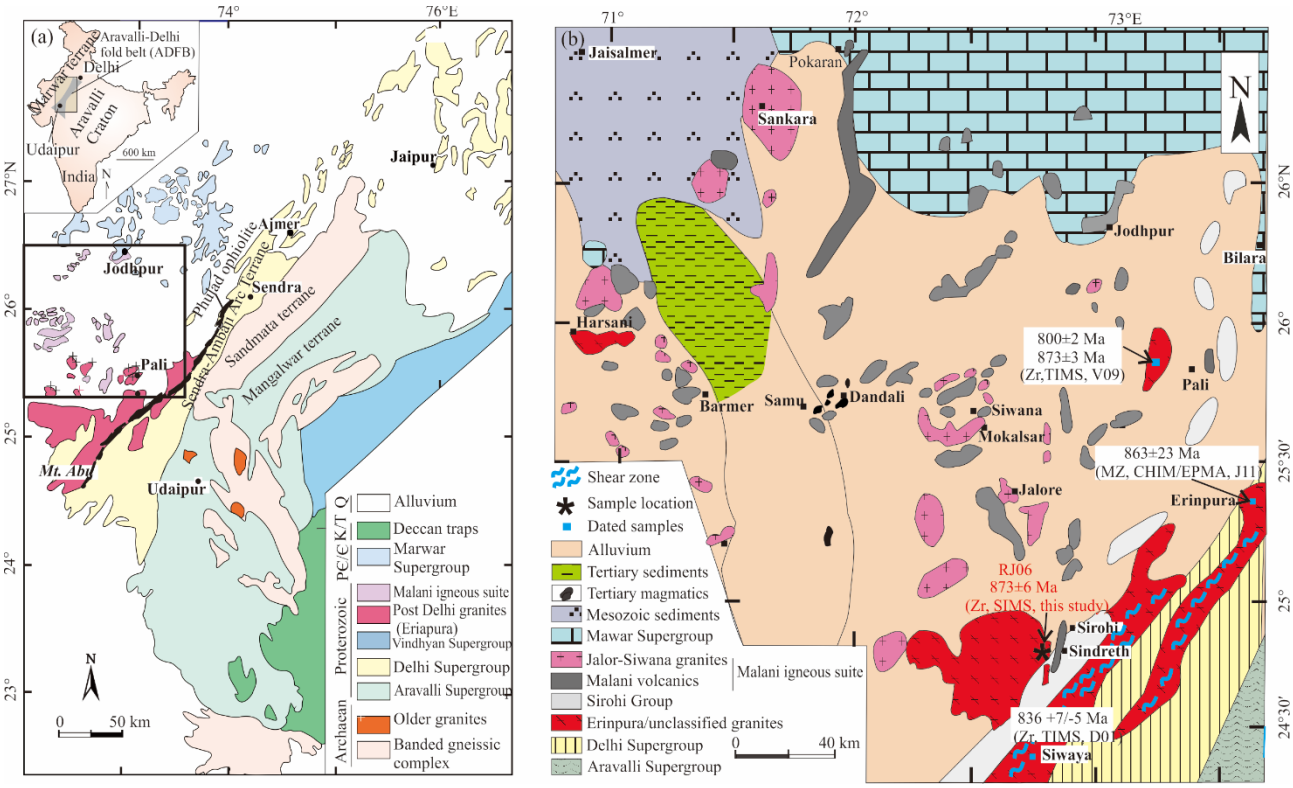

Figure 1. (a) Simplified terrane map showing major units in the NW Indian Block (adapted from Just et al., 2011; van Lente et al., 2009; Roy and Jakhar, 2002). The inset shows the location of the area in India and the rectangle indicates the location of Fig. 1b. (b) Geological map showing the distribution of the Malani Igneous Suite and Erinpura granite in NW India (adapted from Roy and Jakhar, 2002). Data source for cited ages: V09. van Lente et al., 2009; D01. Deb et al., 2001; J11. Just et al., 2011; Zr. zircon; MZ. monazite.

Whole-rock trace element and Nd isotope analyses were conducted at the Institute of Geology and Geophysics, Chinese Academy of Sciences (IGGCAS) in Beijing. Trace elements were analyzed using inductively coupled plasma mass spectrometry (ICP-MS, Perkin-Elmer Sciex ELAN 6100). Sample powders (about 40 mg) were dissolved in high-pressure Teflon bombs using a HF-HNO_3 mixture. An internal standard solution containing the single element Rh was used to monitor signal drift during analysis. A set of USGS standard rocks including BHVO-2, AGV-1, GSR-1, GSR-2, GSR-3, W-2, G-2, SY4, and SARM-4, was chosen as external standards for calibrating element concentrations. The analytical uncertainty precision for most trace elements analysed was <2% (RSD). Reproducibility, based on replicate digestion of samples, is better than 10% (RSD) for most analyses. The overall analytical uncertainty is determined by the investigation of the main sources of uncertainties of the mass spectrometric technique. The relative standard deviation (RSD) was employed to evaluate the stability of the whole analytical method, including sample digestion and instrument measurement. The general laboratory reported uncertainty is the repeated analytical deviation of standard samples as determined by long-term analysis of the standard materials. Analytical accuracy is estimated by the relative deviation between the average value of duplicate analyses of the standards in the long term and published reference values. Regarding the unknown samples, their values are dependent on many factors, including sample homogeneity, sample digestion, instrument stability, and the number of analyses. As the experimental conditions (digestion, sample homogeneity, sample size, instrument parameters, correction method), were uniform, we consider that the unknown samples are also at the same level of analytical accuracy. Analytical accuracy reflects the statistical dispersion of measurement, whereas the analytical uncertainty reflects the deviation of measurement relative to the recommended value (regarded as the 'real' value).

Rock powders for Sm-Nd isotopic analysis were dissolved in Savillex Teflon screw-top capsules after being spiked with mixed ^{149}Sm-^{150}Nd tracers prior to HF+HNO_3+$HClO_4$ dissolution. Sm and Nd were separated using classical two-step ion exchange chromatographic methods and measured using a Triton Plus multi-collector thermal ionization mass spectrometer at IGGCAS. The whole procedural blank was lower than 100 pg for Sm-Nd. Nd isotopic ratios were corrected for mass fractionation by normalizing to $^{146}Nd/^{144}Nd$=0.721 9. The JNdi1 international standard sample was employed to evaluate instrument stability during the period of data collection and the measured value was $^{143}Nd/^{144}Nd$=0.512 115±0.000 010 (n=5, 2SD). USGS reference material BCR-2 was measured to monitor the accuracy of the analytical procedures, with the following results: $^{143}Nd/^{144}Nd$=0.512 634±0.000 009 (n=3, 2SD), which matched well with the recommended value of 0.512 637±0.000 013 (Jweda et al., 2016). The whole-rock major-trace element and Nd isotope data are presented in Table S1.

2.2 *In-situ* Zircon U-Pb-Hf-O Isotope Analysis

Zircon concentrates were separated from ca. 2 kg of rock sample using standard density and magnetic separation techniques. Zircon grains were handpicked and mounted, together with zircon standards TEMORA 2 and BR266, in epoxy mounts that were then polished to section the crystals in half. All zircon grains were imaged in transmitted and reflected light, as well as by cathodoluminescence (CL), to reveal their internal structures. The mount was vacuum-coated with high-purity gold prior to secondary ion mass spectrometry (SIMS) analysis.

Measurements of U, Th and Pb isotopes were undertaken using a CAMECA IMS-1280 large-radius SIMS at IGGCAS. Operating and data processing procedures in this study are similar to those described by Li et al. (2010). The O_2^- primary ion beam was accelerated at 13 kV, with an intensity of about 8 nA. The ellipsoidal spot was about 20×30 μm in size. Positive secondary ions were extracted with a 10 kV potential. Oxygen flooding was used to increase the O_2 pressure to about 5×10^{-6} Torr in the sample chamber, enhancing the secondary Pb^+ sensitivity to a value of about 25 cps/nA/ppm for zircon. In the secondary ion beam optics, a 60 eV energy window was used, together with a mass resolution of about 7 000 (50% peak height), to separate Pb^+ peaks from isobaric interferences. The field aperture was set to 7 000 μm, and the transfer optic magnification was adjusted to 200. Each measurement consisted of 7 cycles, and the total analytical time was about 12 min. A long-term uncertainty of 1.5% (1RSD) for $^{206}Pb/^{238}U$ measurements of the standard zircons was propagated to the unknowns (Li et al., 2010), even though the measured $^{206}Pb/^{238}U$ error during the course of this study was ~1% (1RSD) or less. Data reduction was carried out using the Isoplot/Ex v. 3.0 program (Ludwig, 2003). The external uncertainties of SIMS U-Pb measurements were monitored by inter-calibration of standard zircons BR266 and TEMORA-2. SIMS U-Pb zircon data are listed in Table S2.

The $^{18}O/^{16}O$ ratio in zircons was also measured using a CAMECA IMS-1280 at the IGGCAS. The primary ion beam of $^{133}Cs^+$ was accelerated at 10 kV, with an intensity of ~2 nA. A focused beam of ~10 μm diameter was rastered over 20–30 μm to produce a ~20×20 μm analyzed area. Negative secondary ions were extracted with a -10 kV potential. The normal incidence electron gun was used for charge compensation. Two isotopes of oxygen (^{18}O and ^{16}O) were detected simultaneously using the multi-collector mode with two off-axis Faraday cups (fixed exit slit #2, corresponding to a mass resolution of 2 200). The instrumental mass fractionation was standardized to Vienna Standard Mean Ocean Water composition (VSMOW; $^{18}O/^{16}O$=0.002 005 2) and is reported in standard per mil notation. The internal precision of $^{18}O/^{16}O$ ratios is better than 0.2‰ (2SE) from 20 cycles of measurements. The external reproducibility of $^{18}O/^{16}O$ ratios by repeated measurements of standard zircon TEMORA-2 is better than 0.4‰ (2SD).

Hafnium isotopic compositions of zircon grains were measured using a ThermoFinnigan Neptune MC-ICP-MS equipped with a GeoLas-193 laser ablation system at the IGGCAS. The analytical conditions include an ablation pit of 63 μm diameter (47 μm for small grains), an ablation time of 26 s, a repetition rate of 10 Hz and a laser beam energy density of 10 $J\cdot cm^{-2}$. Laser ablation sites for Hf isotope analysis were centered as close as possible to the spots for previous U-Pb and O isotope analysis, such that the regions of the zircon analysed for both Hf and O isotopes were almost identical in terms of their CL structure.

Calculation of $\varepsilon_{Hf}(t)$ values was based on the Hf chondritic values of Bouvier et al. (2008) and the U-Pb ages of the dated zircon grains. The depleted mantle $^{176}Hf/^{177}Hf$ growth line was calculated

assuming present-day $^{176}Hf/^{177}Hf$=0.283 25, $^{176}Lu/^{177}Hf$=0.038 4 (Griffin et al., 2002) and a decay constant of 1.867×10^{-11} yr^{-1} for ^{176}Lu (Söderlund et al., 2004). The *in-situ* zircon Lu-Hf isotope ratios and $\varepsilon_{Hf}(t)$ values are presented in Table S3.

3 RESULTS

3.1 Whole-Rock Chemical and Nd Isotopic Compositions

Sample RJ06 displays relatively high SiO_2 and K_2O contents (Table S1) and plots in the granodiorite field of the high-K calc-alkaline series on the TAS (K_2O+Na_2O vs. SiO_2) and K_2O vs. SiO_2 diagrams (Figs. 2c, 2d). It is characterized by high K_2O (4.5 %) and Al_2O_3 (15.1%) contents. As shown in Fig. 2, the Erinpura granite data, together with experimental melts, define negative correlations of CaO, TiO_2, MgO, and $Fe_2O_3^T$ with SiO_2 and mol ratios of K/(K+Ca) are also negatively correlated with MgO.

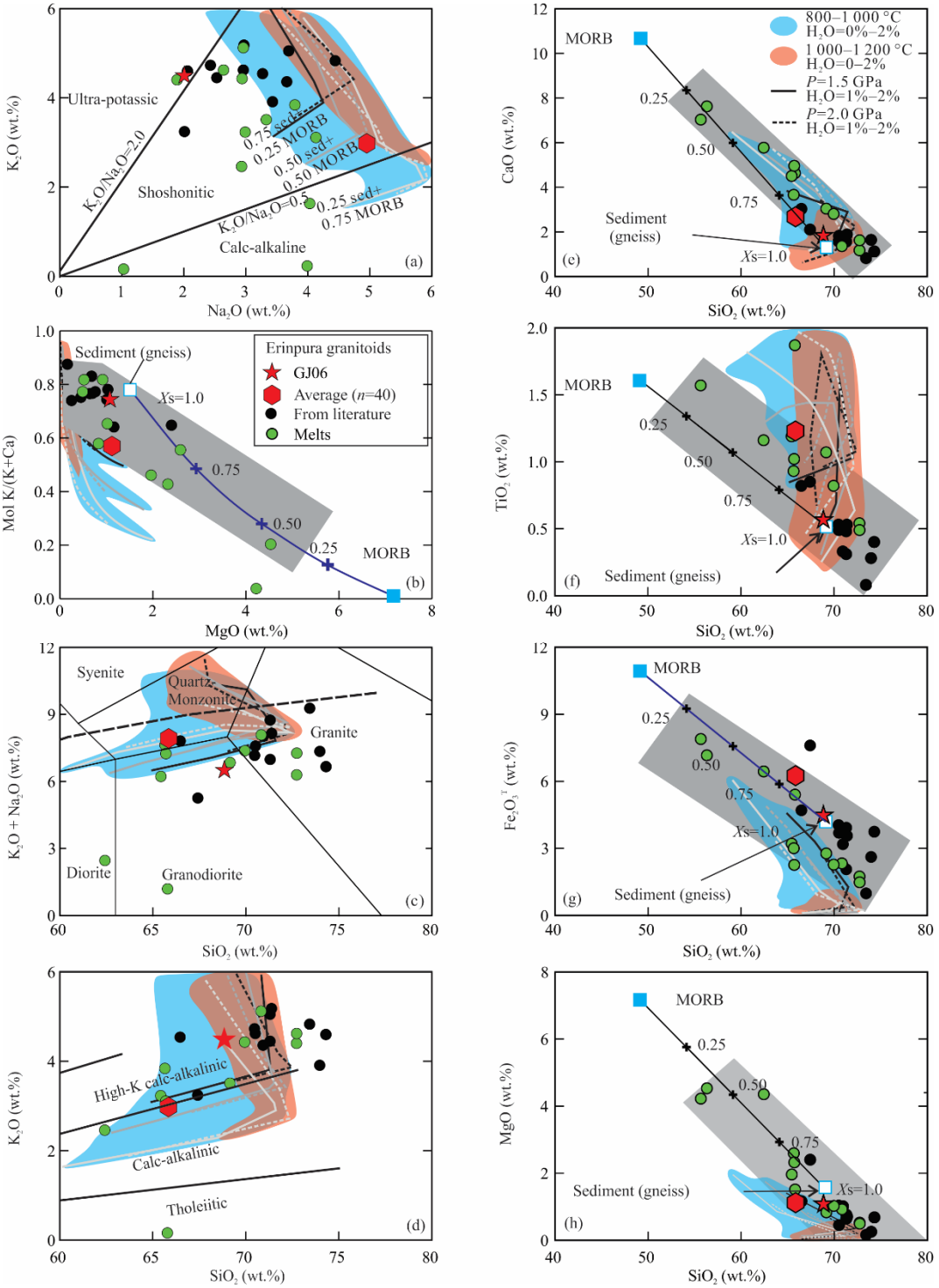

Figure 2. Comparisons of experimental melts derived from a mixture of MORB+sediments (Castro et al., 2010) and the studied granite (RJ06, red star). (a) K_2O versus Na_2O (wt.%); (b) molar ratio K/(K+Ca) vs. MgO (wt.%); (c) Na_2O+K_2O vs. SiO_2 (wt.%); (d) K_2O vs. SiO_2 (wt.%); (e) CaO vs. SiO_2 (wt.%); (f) TiO_2 vs. SiO_2 (wt.%); (g) $Fe_2O_3^T$ vs. SiO_2 (wt.%); and (h) MgO vs. SiO_2.

In Fig. 2, the red hexagon indicates the average value of Erinpura granodiorite that was estimated from the 40 samples analysed by Naik (1993). The other Erinpura granodiorite data are from Solanki (2011). *X*s indicates the fraction of sedimentary component in the mixture of MORB+sediments. The contributions of melting temperature, pressure and source region were estimated using alpha MELTS (Smith and Asimow, 2005), as shown by blue and light pink areas and solid and dashed lines. The blue and light pink areas indicate the effect of melting temperature on melt compositions. The modelling results show that the controlling factors are melting temperature and source heterogeneity. Melting pressure contributes less to the composition of the calculated melts. The contributions of source region and melting pressure to melt compositions are also shown by solid (P=2.0 GPa) and dashed (P=1.5 GPa) lines at H_2O=1.0 wt.%–2.0 wt.%. White, grey, and black solid and dashed lines indicate calculated melts for starting materials of 0.75MORB+0.25sediment, 0.5MORB+0.5sediment, and 0.25MORB+0.75 sediment, respectively.

The granite shows a LREE-enriched chondrite-normalized REE pattern with La_N=243, Yb_N=28.9, and La_N/Yb_N=8.1 and a strong negative Eu anomaly ($Eu/Eu^*=(Gd_N)^{1/2}/[(Sm_N)^{1/2}\times(Gd_N)^{1/2}]$ =0.48; Fig. 3a). This pattern is typical of magmatic rocks developed in an arc environment (Condie and Baragar, 1974). The presence of a strong negative Eu anomaly indicates that crystal fractionation of feldspars may have played a significant role in its magmatic evolution. This is consistent with depletion of Sr (Fig. 3b) in the primitive mantle-normalized incompatible trace element spidergram, which also reveals enrichment in Rb, Ba, Th, U, and LREE and depletion in Nb and Ta.

The sample has mantle-like $^{143}Nd/^{144}Nd$ and $^{147}Sm/^{144}Nd$ isotope ratios of 0.512 041 and 0.124 7, respectively, corresponding to an $\varepsilon_{ND}(t)$ value of +3.5 (Table S1).

3.2 Zircon Dating and Hf-O Isotopic Analysis

Zircon grains used for U-Pb dating are mostly euhedral to subhedral, ~100 to 250 μm long, with length to width ratios of 3 : 1 to 5 : 1. Twenty analyses were conducted on 20 grains (Table S2) and recorded high U (405 ppm−8 569 ppm) and Th (91 ppm–1 003 ppm) contents, which can be divided into relatively low-U (405–973) and high-U subgroups (>1 000 ppm, up to 8 569 ppm). Oscillatory zoning is common in most grains (Fig. 4) and, together with high Th/U ratios (0.12–0.48), indicate a magmatic origin. With the exception of high common lead in spot #1 (3.4% ^{204}Pb; Table S2) and spot #4 (high-U and large degree of discordance; Table S2), the other eighteen analyses yield a weighted mean $^{206}Pb/^{238}U$ age of 893±6 Ma (MSWD=0.72, 95% confidence interval). With the removal of only the high common lead analysis spot #1, the other nineteen analyses yield a weighted mean $^{207}Pb/^{206}Pb$ age of 873±6 Ma (MSWD=0.66, n=19), which is similar to the concordia $^{207}Pb/^{206}Pb$ age of 886±6 Ma (MSWD=14) considering the analytical uncertainty (Fig. 5).

The twenty sites used for U-Pb dating were also measured for $\delta^{18}O$ and they vary from 8.1‰ to 10.3‰. The $\delta^{18}O$ values record two populations, with a dominant peak at +9.9‰ and a minor peak at +8.9‰ (Fig. 6a and Table S3). The twenty analyses have uniform $^{176}Hf/^{176}Hf$ isotope ratios of 0.282 482 to 0.282 526. Because no inherited zircon grains were recognized in this study and the zircons all contained high concentrations of U, we used the weighted mean $^{207}Pb/^{206}Pb$ age (873 Ma) to calculate the initial Hf isotopes with $\varepsilon_{Hf(873\ Ma)}$=+9.3 to +10.9 (Fig. 6b).

4 DISCUSSION

4.1 Effect of U-Pb Disturbance and High U Concentrations on Zircon U-Pb Age and Oxygen Isotope

As shown in Fig. 5, the analysed zircon grains show slight U-Pb reverse discordance, due to the high U content of the zircon grains. It is widely-known that high-U zircon grains commonly yield apparently older U-Pb ages (White and Ireland, 2012) and lower oxygen-isotope values (Booth et al., 2005) in ion microprobe analyses. Thus, high-U zircon grains maybe variably depleted in ^{18}O (Booth et al., 2005). Therefore, before using zircon U-Pb-O data to investigate the petrogenesis of the granitoid, we evaluated the effects of U-Pb disturbance and high-U concentrations on apparent zircon U-Pb ages and oxygen isotopic composition.

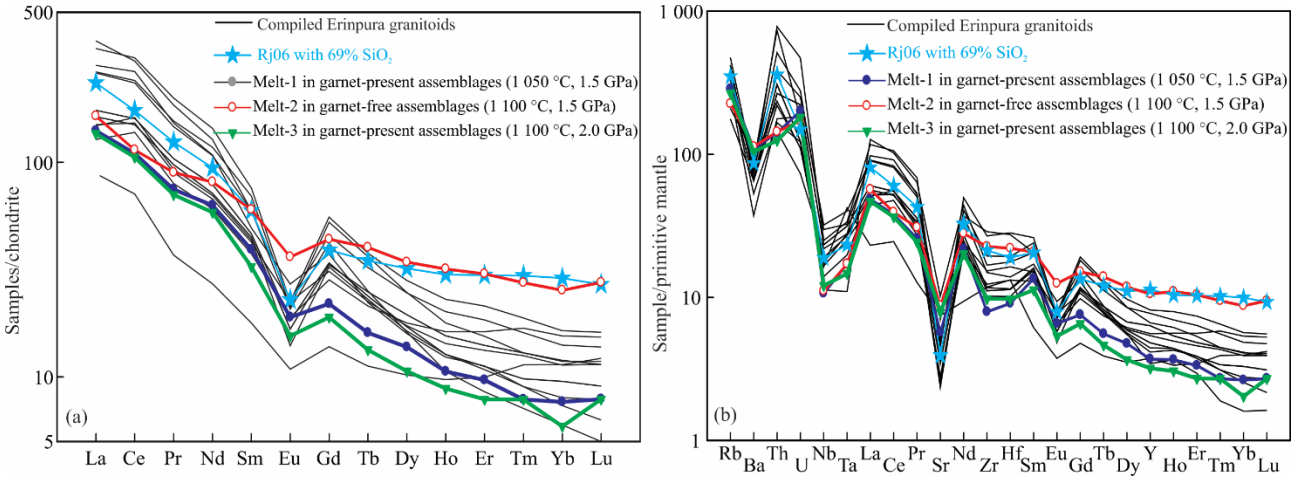

Figure 3. (a) REE-chondrite normalized patterns and (b) primitive mantle-normalized incompatible trace element spidergram for granite sample RJ06 and experimental melts: normalization values are from Sun and McDonough (1989). Experimental melt data are from Castro et al. (2010) and the other Erinpura granodiorite data are from Solanki (2011).

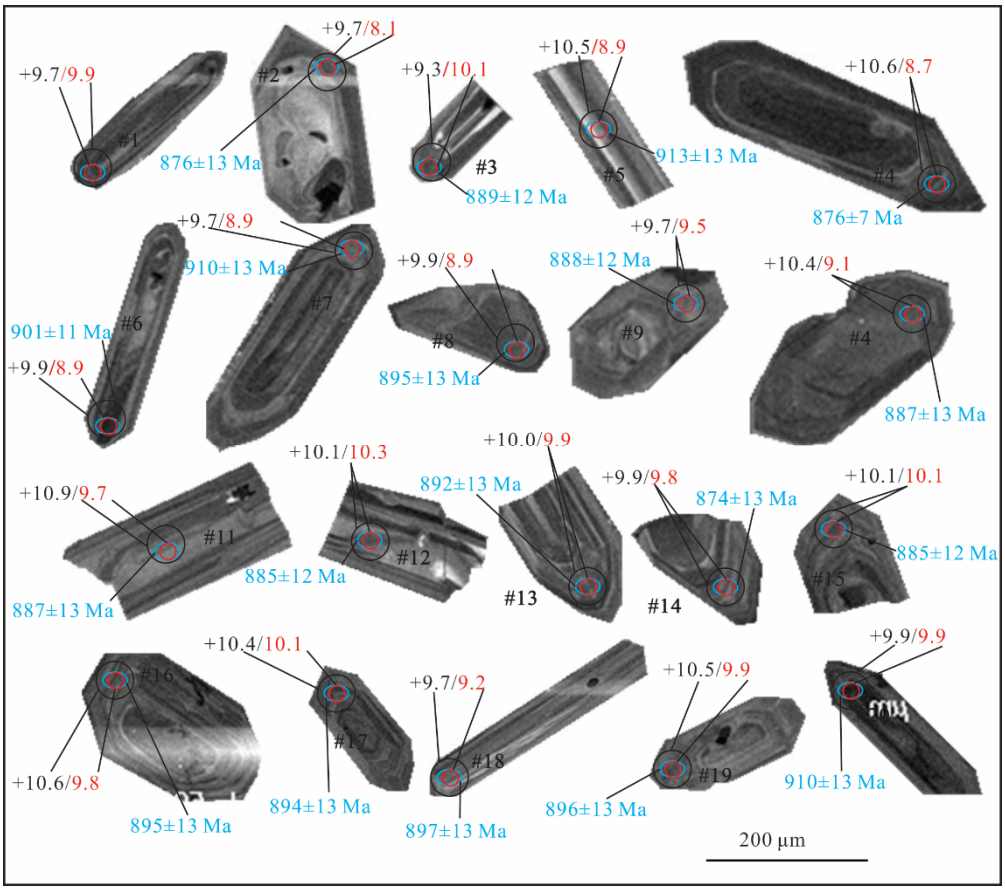

Figure 4. Cathodoluminescence (CL) images of typical zircons from granitoid sample RJ06. The small blue and red ellipses represent the sites of SIMS U-Pb and O isotope analyses, respectively; the large black circles represent the sites of LA-MC-ICPMS Hf isotope analyses. The numbers in blue, red, and black are the U-Pb dates (Ma), $\delta^{18}O$, and $\varepsilon_{Hf}(t)$, respectively.

The apparent $^{206}Pb/^{238}Pb$ ages are broadly positively correlated with *D* (percentage discordance, %) values (Fig. 7a). Furthermore, spots #4, #7, and #20, the three high-U zircon grains (analysis spot #1 was already discarded due to its high common lead) display older $^{206}Pb/^{238}Pb$ ages (inset in Fig. 7b), whereas low-U zircon grains show no change (Fig. 7b). Therefore, the $^{207}Pb/^{206}Pb$ ages are considered more reliable. Thus, the weighted mean $^{207}Pb/^{206}Pb$ age of 873±6 Ma (MSWD=0.66, n=19) represents the best estimate of the crystallisation age of the granite.

As shown in Fig. 7c, there is no meaningful correlation between the measured zircon $\delta^{18}O$ values and the degree of U-Pb discordance (*D* values), although there is a distinct separation into two populations with minimal overlap. The lack of correlation implies that high-U radiation damage did not have a significant effect on the zircon oxygen signatures. Neither do the low-U (<1 000 ppm) or high-U (≥1 000 ppm) zircon grains display any correlation between measured zircon $\delta^{18}O$ values and U concentrations (Fig. 7d). This suggests that radiation damage because of high U concentration did not result in lower oxygen-isotope values. Although the highest-U grain (#spot#4) displays a low $\delta^{18}O$ value, no change in oxygen isotope composition is distinguishable in the remaining set of 19 zircons, considering the 0.5‰ of external standard error (2σ for *in-situ* SIMS zircon oxygen analysis (Fig. 7d). This likewise implies that the zircon oxygen isotopes are not disturbed. Thus, the high zircon $\delta^{18}O$ value is a primary feature of the granite.

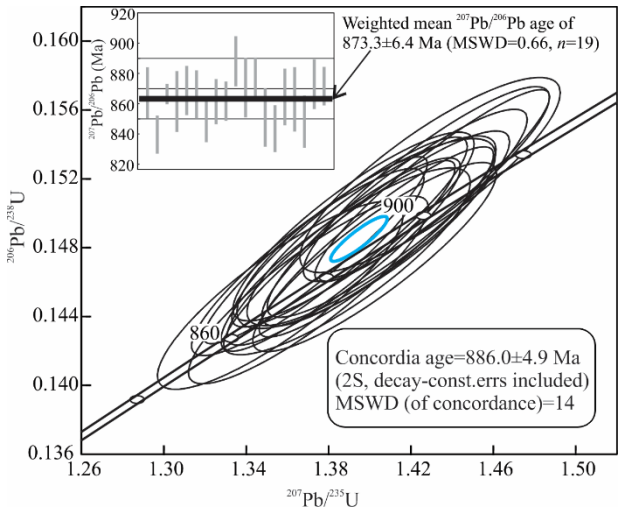

Figure 5. U-Pb concordia diagram for granitoid sample RJ06. Ages are in Ma and ellipses have 1σ errors. Inset figure shows data used to define the weighted mean $^{207}Pb/^{206}Pb$ age. Percentage discordance *D* is defined as $(e^{\lambda 235\times T7/6}-1)>^{207}Pb/^{235}U_m$, $D=((e^{\lambda 235\times T7/6}-1)-^{207}Pb/^{235}U_m)^2+((e^{\lambda 238\times T7/6}-1)-^{206}Pb/^{238}U_m)^{0.5}/((^{207}Pb/^{235}U_m)^2+(^{206}Pb/^{238}U_m)^2)^{0.5}$, or $D=-((e^{\lambda 235\times T7/6}-1)-^{207}Pb/^{235}U_m)^2+((e^{\lambda 238\times T7/6}-1)-^{206}Pb/^{238}U_m)^{0.5}/((^{207}Pb/^{235}U_m)^2+(^{206}Pb/^{238}U_m)^2)^{0.5}$, where m and *T*7/6 indicate measured values and $^{207}Pb/^{206}Pb$ age, respectively. The decay constant is: $\lambda 235=9.848\ 50\times10^{-10}$, $\lambda 238=1.551\ 25\times10^{-10}$.

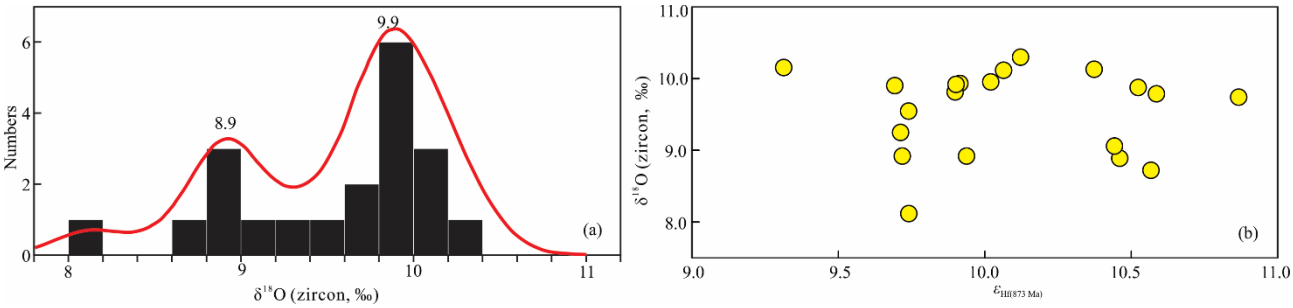

Figure 6. (a) Histogram of zircon $\delta^{18}O$ values and (b) $\varepsilon_{Hf}(t)$ vs. $\delta^{18}O$ values for the ca. 873 Ma granite sample RJ06.

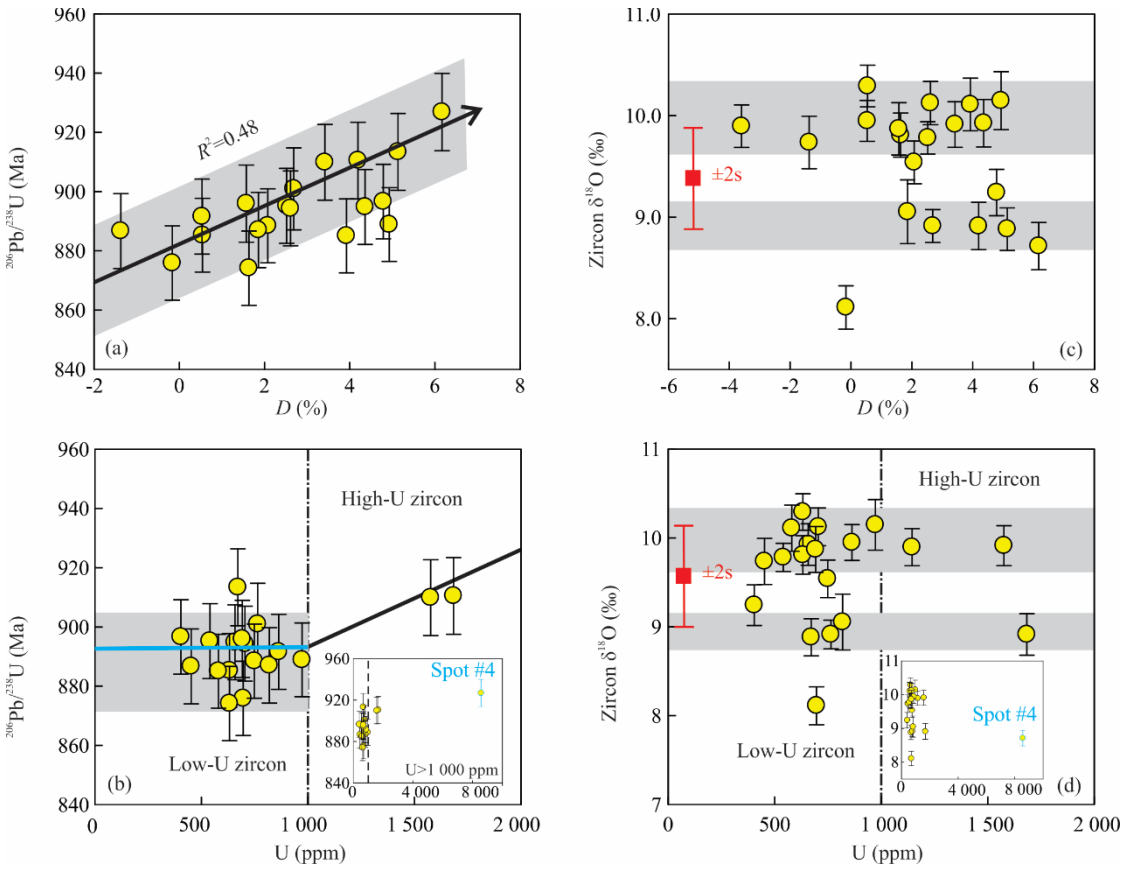

Figure 7. Plots of $^{206}Pb/^{238}U$ age vs. (a) discordance and (b) U concentration, and zircon $\delta^{18}O$ values against (c) discordance and (d) U concentration.

4.2 Hf-Nd Isotopic Systematics

The most prominent feature of the granite data is the decoupling between radiogenic Hf-Nd and O isotopes. Zircon grains show high positive and homogenous $\varepsilon_{Hf(873Ma)}$ values of +9.3 to +10.9, plotting along the new continental crustal growth curve as defined by modern island arc basalt (Fig. 8). This is consistent with the mantle-like whole-rock Nd isotope composition with an $\varepsilon_{Nd(873\ Ma)}$ value of +3.6. The average zircon $\varepsilon_{Hf(873\ Ma)}$ and whole-rock $\varepsilon_{Nd(873\ Ma)}$ values also plot on the juvenile modern arc array in the ε_{Hf}-ε_{Nd} diagram (Fig. 9a). This implies that the granite has juvenile Nd-Hf isotopic compositions, and thus represents addition of juvenile materials to the continental crust (Fig. 9). However, its zircon grains show high $\delta^{18}O$ values of 8.1‰ to 10.3‰, significantly higher than that of the pristine mantle zircon value of 5.3‰±0.3‰ (Valley et al., 1998). The whole-rock $\delta^{18}O$ values were calculated as 9.8‰ to 11.9‰, with an average of 11.3‰±0.6 ‰, based on SiO_2 contents and using the equation of $\delta^{18}O_{WR} \approx \delta^{18}O_{Zir}+0.061\ 2\ (wt.\%\ SiO_2)-2.5$ (Valley et al., 2005). The calculated whole-rock values straddle the range in $\delta^{18}O$ values of typical I-type ($\delta^{18}O$=6‰–10‰) and S-type ($\delta^{18}O$=10‰–14‰; Eiler, 2001) granites. Such a high $\delta^{18}O$ value is generally a supracrustal signature (Valley et al., 2005) and can be either attributed to crustal contamination or to a source region that contains hydrothermally-altered surface components. Contributions from supracrustal rocks that show high $\delta^{18}O$ values varying from 10‰ to 35‰ (Bindeman et al., 2005) have the potential to significantly increase the $\delta^{18}O$ value of parental magmas. However, the supracrustal zircon O isotope signature requires >30% sediment contribution in the source (sediment end-member with $\delta^{18}O$=20‰ and parental magma with $\delta^{18}O$=6‰). The input of such a high proportion of sediments should significantly modify both the Hf and Nd isotope compositions of the resultant magma. This may also result in the presence of abundant xenocrystic zircon grains and generate a

large range of zircon Hf isotope values. This is inconsistent with the observation of homogeneous, mantle-like zircon Hf isotopes, the absence of xenocrystic zircon grains and mantle-like whole-rock Nd isotope composition of the Erinpura granite. This implies that the observed decoupling between mantle-like Nd-Hf and supracrustal O isotopes most likely reflects a source region that contained, or was dominated by, hydrothermally-altered juvenile components.

4.3 Decoupling between Zircon Oxygen and Hafnium Isotopes: Implication for Melting of Subducted Oceanic Basalts and Sediments Leading to Juvenile Crustal Growth

The decoupling between Nd-Hf and O isotopes can be generated by partial melting of metasomatized sub-arc mantle or hydrothermally-altered upper oceanic crust. Plate subduction continuously transports crustal materials with high-$\delta^{18}O$ values down into the mantle wedge, where high-$\delta^{18}O$ features may be transferred to mantle peridotite by dehydration and partial melting processes (Liu et al., 2014; Eiler et al., 2007). High-$\delta^{18}O$

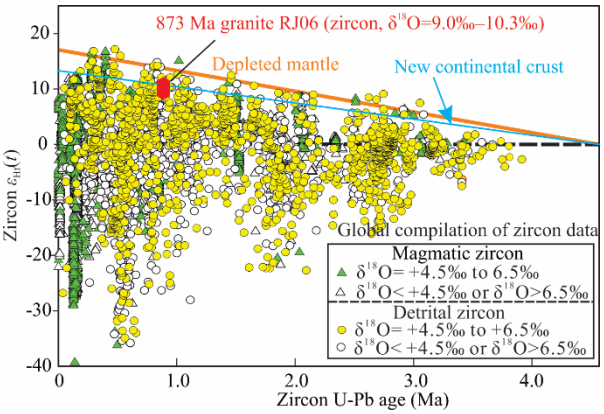

Figure 8. Plot of $\varepsilon_{Hf}(t)$ vs. U-Pb age for magmatic and detrital zircon grains with different $\delta^{18}O$ values. The depleted mantle growth curve is drawn with present day ε_{Hf}= +17 projected back to 4.5 Ga (Griffin et al., 2000). The new continental crustal growth curve is drawn with present day ε_{Hf}= +13.2 as in modern island arcs (Dhuime et al., 2011) and projected back to zero at T=4.5 Ga. The global zircon data source is presented in Appendix A.

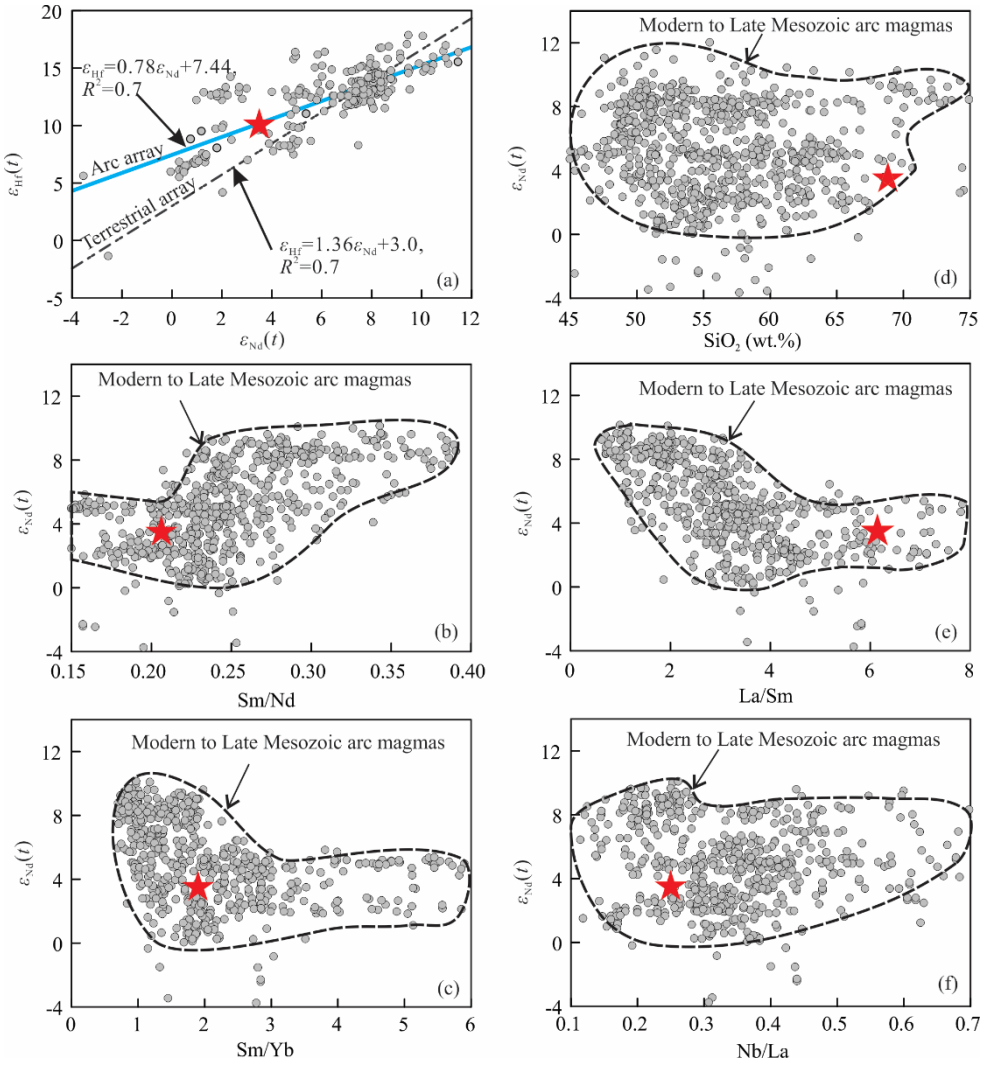

Figure 9. Plots of (a) $\varepsilon_{Hf}(t)$ vs. $\varepsilon_{Nd}(t)$, (b) $\varepsilon_{Nd}(t)$ vs. Sm/Nd, (c) $\varepsilon_{Nd}(t)$ vs. Sm/Yb, (d) $\varepsilon_{Nd}(t)$ vs. SiO_2, (e) $\varepsilon_{Nd}(t)$ vs. La/Sm, and (f) $\varepsilon_{Nd}(t)$ vs. Nb/La for sample RJ06 (red star) and modern to Late Mesozoic arc magmas from the Banda arc, the Lesser Antilles, the Izu-Bonin intra-oceanic arc, the Aleutian arc, the Japan arc, the Nascent arc (Reagan et al., 2008), the Central Mexican volcanic belt, the Sunda arc, the intra-oceanic Kermadec arc, the Lassen continental arc, the Kamchatka arc, and the Andes arc. The arc and terrestrial arrays are from Vervoort et al. (2011). The data sources are presented in Appendix A.

values ranging from 8.8‰ to 11.3‰ have been documented in silica-rich glass/melt inclusions entrained in peridotite xenoliths from island arcs (Eiler et al., 2007), which have been interpreted as low-degree melts from refractory mantle metasomatized by slab-derived fluids/melts. Recent identification of high $\delta^{18}O$ values ($\delta^{18}O_{olivine}$=8.03±0.28‰) in the Sailipu mantle xenoliths from southern Tibet demonstrates that some portions of the sub-arc lithospheric mantle have $\delta^{18}O$ values significantly higher than the upper mantle (Liu et al., 2014). Thus, partial melting of high-$\delta^{18}O$ sub-arc mantle has the potential to produce the observed decoupling between Hf-Nd and O isotopes. However, because such mantle reservoirs have refractory compositions (Liu et al., 2014), melting requires high water influx and the resultant melts are high in magnesium and compatible trace elements and relatively low in silica, with basaltic to andesitic composition, such as boninite and high-Mg andesite. This is inconsistent with the low magnesium and granitic major element composition of the granite in this study.

The Hf-Nd isotope composition of the studied granite is similar to young arc magmas, as evidenced by its plotting on the arc array defined by modern to Late-Mesozoic arc magmas in Hf-Nd isotope space (Fig. 9a). Its Nd isotope, trace element ratios (Sm/Nd, Sm/Yb, La/Sm and Nb/La) and major elements (e.g., SiO_2) also show strong affinities with young arc magmas (Figs. 9b–9f). This is consistent with the geological constraint that the Erinpura granitoids represent the syn- to late orogenic phase of magmatism formed during the Delhi orogeny, corresponding to the final assembly of the supercontinent Rodinia. This is supported by the variations in the deformation from pristine igneous to gneissic (Just et al., 2011; Pandit et al., 2003; Deb et al., 2001; Naik, 1993; Choudhary et al., 1984). Thus, the Erinpura granitoids have been widely proposed to be produced in an Andes-type subduction environment. The Erinpura granitoids are also closely associated in space and time with an active continental margin related to subduction. As shown in Fig. 10, young arc magmas are characterized by large ranges in whole-rock $\delta^{18}O$ values, varying from about +4‰ to >+12‰. Furthermore, some young juvenile arc crust with $SiO_2 \leq 60$ wt.% and $\varepsilon_{Nd}(t)>0$ displays strongly supracrustal $\delta^{18}O$ signatures (>+7‰). This implies that the decoupling between Nd-Hf and O isotopes observed in the granite can be produced within an arc environment. In summary, the lines of evidence presented in this study suggest an arc setting for the origin of the Erinpura granitoids.

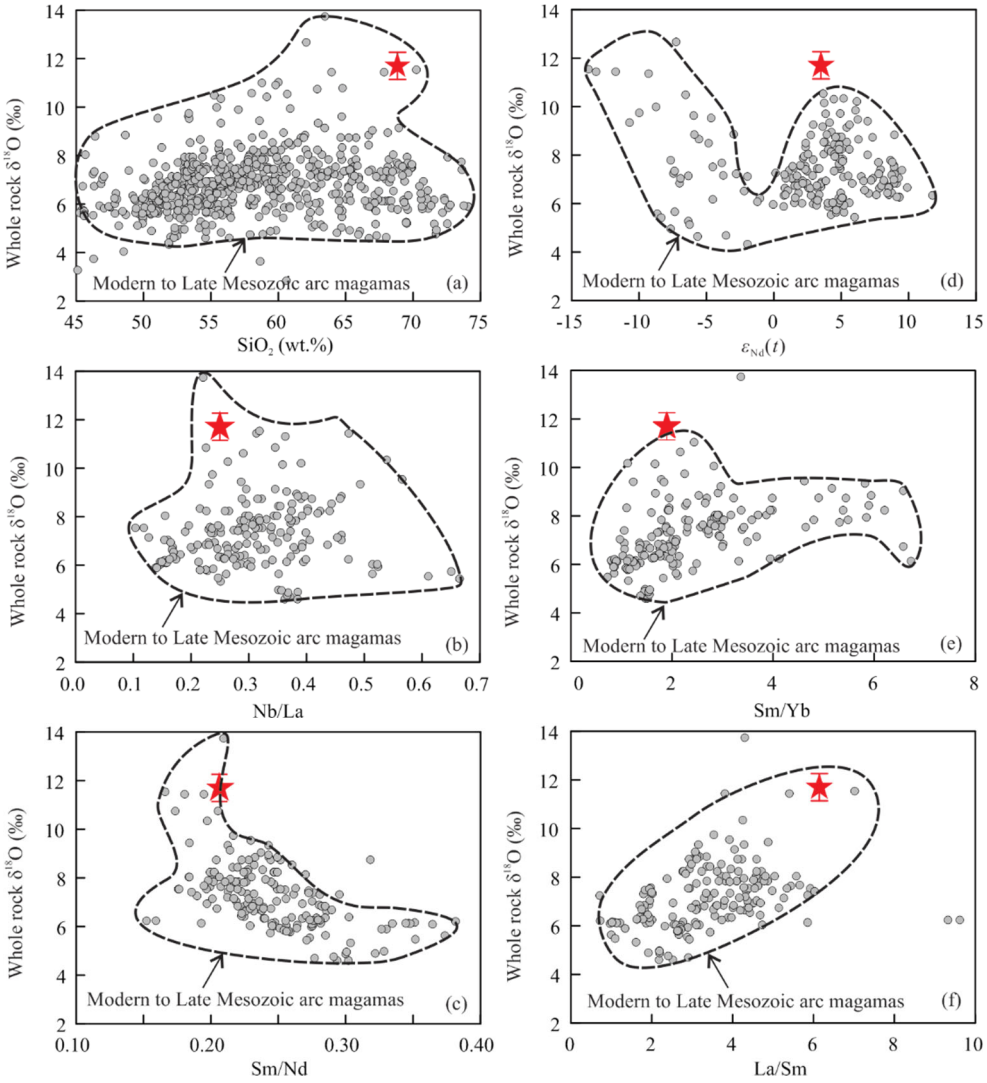

Figure 10. Plots of calculated whole-rock $\delta^{18}O$ values against (a) SiO_2, (b) Nb/La, (c) Sm/Nd, (d) $\varepsilon_{Nd}(t)$, (e) Sm/Yb, (f) La/Sm for sample RJ06 (red star) and modern to Late Mesozoic arc magmas. The data sources are the same as in Fig. 9.

Experimental (Behn et al., 2011; Castro et al., 2010), numerical modelling (Castro et al., 2013; Zhu et al., 2013) and geochemical (Niu et al., 2013; Gómez-Tuena et al., 2008; Kelemen, 1995) studies indicate that melting of the slab and associated diapirism may be the rule rather than the exception beneath the arc front in most subduction zones (Behn et al., 2011), and that this mechanism can produce melts that strongly resemble andesitic arc magmas (Castro et al., 2010). Recent four-dimensional numerical modelling proposes that melts derived from subducted oceanic crust and sediments could contribute up to 15 vol.%–50 vol.% to arc crust (Zhu et al., 2013).

Surface water-rock interaction mainly modifies the O isotopes and has little effect on the radiogenic (Hf-Nd) isotope compositions of oceanic crust. Additionally, the short residence time ensures that melts derived from subducted oceanic crust have mantle-like radiogenic (Hf-Nd) isotope compositions. Therefore, juvenile continental crust formed by partial melting of upper oceanic crust (a mixture of MORB+sediments) should possess mantle-like Hf-Nd and a supracrustal O isotope signature. Hence, the observed decoupling between Hf-Nd and O isotopes may indicate that the source of the studied granite from NW India was hydrothermally-altered upper oceanic crust and sediments. This is consistent with the calculated whole-rock $\delta^{18}O$ values of 11.3‰±0.6‰, which matches that of hydrothermally-altered upper oceanic crust (generally ranging from 7‰ to 15‰; Eiler, 2001), and the peak value observed from pillow lavas and sheeted dykes from ophiolites (Fig. 11). Moreover, the whole-rock major element composition of the granite is comparable to experimental melts derived from a mixture of MORB-derived amphibolite and sediments at temperatures of 1 000–1 200 °C and pressures of 1.5–2.0 GPa (Figs. 2, 3). Trace element distribution patterns of the granite are similar to those of experimental melts in garnet-free assemblages at a somewhat lower pressure (1.5 GPa), but display relatively higher heavy rare earth element (HREE) contents than those of melts of garnet-present assemblages (Fig. 3). Taken together with the decoupling between Nd-Hf and O isotopes, the parental magma of the granite was most likely generated by partial melting of a mixture of MORB+sediment at a relatively low pressure (1.5 GPa).

The published data for the Erinpura granitoids, including sample GJ06, share similar trends with experimental melts, characterised by negative trends of CaO, MgO, TiO_2, and $Fe_2O_3^T$ versus SiO_2, and MgO vs. mol. ratio of K/(K+Ca) (Fig. 2). Both natural samples and experimental melts plot within or along the mixing trend defined by MORB and sediments. Partial melting simulation results by alpha MELT (Smith and Asimow, 2005) show that melting temperature and source heterogeneity are controlling factors for melt composition. The least controlling factor for melt composition is melting pressure. When water content in the source region is not more than 1.0 wt.%, its contribution can be ignored. As shown in Fig. 2, simulation results suggest that partial melting of a mixture of MORB plus variable sediment at temperatures of 1 000–1 200 °C and pressure of 1.5 GPa with H_2O=1.0 wt.%–2.0 wt.% can produce the features observed in the Erinpura granitoid suite. This is also supported by the experimental results (Figs. 2, 3) and the presence of garnet in the residue (Fig. 12).

The Erinpura granodiorites exhibit a wide spectrum of REE patterns from strongly fractionated to unfractionated. Some granodiorites plot in the garnet-free region of the diagram, whereas many others appear to be produced from a source in equilibrium with garnet. In general, the REE distribution patterns (Fig. 3) and contents (Fig. 12) for the Erinpura granitoids can be compared to those of melts of a mixture of MORB and sediments. The difference between natural samples and experimental melts may be partially attributed to the variation in pressure and/or temperature of partial melting (Castro et al., 2010). Because the experimental results show that melts developed at higher temperature have a greater probability of being generated in a garnet-free environment compared with lower temperature melts, the more depleted HREE patterns are therefore expected to be the result of fractionation at lower melting temperature from the same source. The variability of subducted oceanic crust (igneous crust end-member+sediment end-member) would also contribute to the difference between the natural samples and experimental melts.

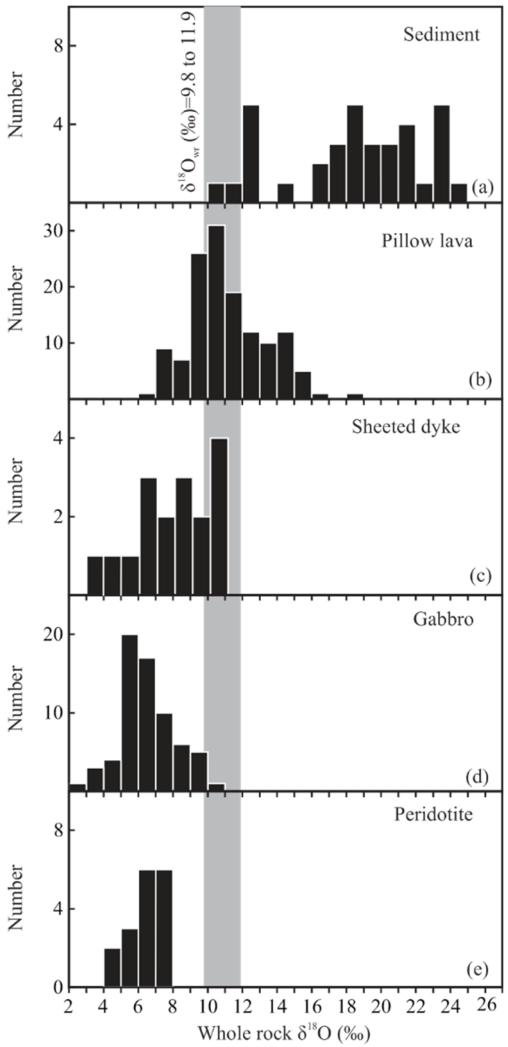

Figure 11. Histograms of whole-rock $\delta^{18}O$ values of (a) sediments, (b) pillow lavas, (c) sheeted dykes, (d) gabbro, and (e) peridotite from the Corsican and Oman ophiolites. The range of calculated whole-rock $\delta^{18}O$ matches well with the majority of pillow lavas and overlaps with the highest value for the sheeted dykes. The data were compiled from Miller et al. (2001) and Yamaoka et al. (2012).

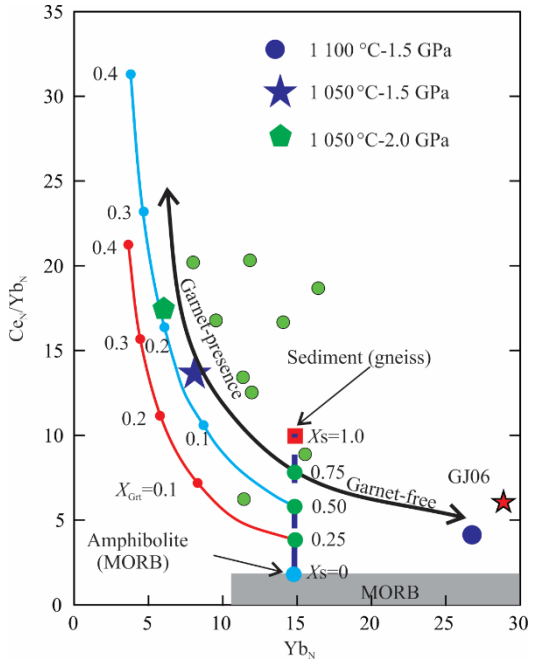

Figure 12. Comparing Ce_N/Yb_N vs. Yb_N of experimental melts with the Erinpura granodiorite. Two model lines correspond to a mixture with a fraction of sediments (*Xs*) of 0.25 and 0.5 and show the progressive depletion in HREE (dashed line) in the melt as a function of the amount of garnet (Grt) in the system (Castro et al., 2010). Numbers on the evolution lines indicate the fraction of garnet left in the residue. Subscript N indicates chondrite-normalized values. The modelling results and experimental melts are from Castro et al. (2010). Green dots indicate the additional Erinpura granodiorite data, which are from Solanki (2011).

According to the results of our numerical modelling and comparison with experimental melts, partial melting of a mixture of basalt and sediment at a temperature of 1 000–1 200 °C and a pressure of 1.5 GPa with moderate H_2O of 1.0 wt.%–2.0 wt.% can generate the Erinpura granitoids. Because the tectonic setting of the Erinpura granitoids is from the late-stage of the Delhi orogeny (Grevillian orogenic event) to the earliest phase of the breakup of Rodinia (Wu et al., 2018; Lyu et al., 2017), this stage likely corresponds to the earliest phase of mantle upwelling that initiated the breakup (Wang et al., 2016), thus providing a mechanism to melt mixtures of basalt plus sediment to produce juvenile continental crust (cf. Castro et al., 2013, 2010).

The above observations show that decoupling between Hf-Nd and O isotopes in high-silica magmas is a diagnostic feature for identifying a contribution from subducted upper oceanic crust in generating juvenile continental crust. It is widely accepted that the growth of continental crust during the Archean involved relatively large contributions from slab melts (e.g., Martin et al., 2005; Rapp et al., 2003; Foley et al., 2002). Archean tonalite-trondhjemite-granodiorite (TTG) suites represent preserved early juvenile continental crust (3.8–2.5 Ga) and are the most plausible candidates for these slab melts and their differentiation products in the Archean (Moyen and Martin, 2012; Martin et al., 2005; Rapp et al., 2003). Zircon grains from Archean TTG display high $\delta^{18}O$ values of 6.5‰–7.5‰, which were interpreted to result from interaction of the amphibolite protolith with surface waters at low temperature, followed by melting or contamination to create mildly elevated magmas that host the zircons (Valley et al., 2005). Thus, the co-existence of juvenile Nd-Hf isotopes and high $\delta^{18}O$ values in Archean TTG suites provides the key evidence for slab melting during early continental crustal growth.

5 CONCLUSIONS

A ca. 870 Ma granitoid from NW India displays mantle-like zircon Hf ($\varepsilon_{Hf(873\ Ma)}$= +9.3 to +10.9) and whole-rock Nd ($\varepsilon_{Nd(873\ Ma)}$= +3.5) characteristics, but supracrustal zircon $\delta^{18}O$ values, mostly ranging from 9‰ to 10‰. The observed decoupling between radiogenic and oxygen isotopes indicates that the protolith was juvenile material modified by surface water-rock interaction under low temperature conditions. Furthermore, the major-trace element composition of the granite is similar to that of experimental melts produced by partial melting of a mixture of MORB+sediments. Thus, the decoupling between mantle-like radiogenic Nd-Hf isotopes and supracrustal O isotopes may be used as a key diagnostic feature for the identification of contributions from subducted oceanic crust to juvenile crustal growth. Our results therefore suggest that partial melting of subducted oceanic basalts (plus sediments) may have played an important role in early continental crustal growth.

ACKNOWLEDGEMENTS

This work was supported by the National Key R & D Program of China (No. 2017YFC0601302), the Research Start-up Project for Introduced Talent of Yunnan University (No. 20190043), and the Australian Research Council grants to Zheng-Xiang Li (Nos. DP0770228, FL150100133). We would like to express special thanks to editor for handling the manuscript and three anonymous reviewers for their constructive comments. The final publication is available at Springer via https://doi.org/10.1007/s12583-020-1095-2.

Electronic Supplementary Materials: Supplementary materials (Tables S1, S2, S3) and Appendix A are available in the online version of this article at https://doi.org/10.1007/s12583-020-1095-2.

REFERENCES CITED

Solanki, A. M., 2011. A Petrographic, Geochemical and Geochronological Investigation of Deformed Granitoids from SW Rajasthan: Neoproterozoic Age of Formation and Evidence of Pan-African Imprint: [Dissertation]. University of the Witwatersrand, Johannesburg

Ashwal, L. D., Solanki, A. M., Pandit, M. K., et al., 2013. Geochronology and Geochemistry of Neoproterozoic Mt. Abu Granitoids, NW India: Regional Correlation and Implications for Rodinia Paleogeography. *Precambrian Research*, 236: 265–281. https://doi.org/10.1016/j.precamres.2013.07.018

Behn, M. D., Kelemen, P. B., Hirth, G., et al., 2011. Diapirs as the Source of the Sediment Signature in Arc Lavas. *Nature Geoscience*, 4(9): 641–646. https://doi.org/10.1038/ngeo1214

Bindeman, I. N., Eiler, J. M., Yogodzinski, G. M., et al., 2005. Oxygen Isotope Evidence for Slab Melting in Modern and Ancient Subduction Zones. *Earth and Planetary Science Letters*, 235(3/4): 480–496. https://doi.org/10.1016/j.epsl.2005.04.014

Bouvier, A., Vervoort, J. D., Patchett, P. J., 2008. The Lu-Hf and Sm-Nd Isotopic Composition of CHUR: Constraints from Unequilibrated Chondrites and Implications for the Bulk Composition of Terrestrial Planets. *Earth and Planetary*

Science Letters, 273(1/2): 48–57. https://doi.org/10.1016/j.epsl.2008.06.010

Buick, I. S., Clark, C., Rubatto, D., et al., 2010. Constraints on the Proterozoic Evolution of the Aravalli-Delhi Orogenic Belt (NW India) from Monazite Geochronology and Mineral Trace Element Geochemistry. *Lithos*, 120(3/4): 511–528. https://doi.org/10.1016/j.lithos.2010.09.011

Castro, A., Gerya, T., Garcia-Casco, A., et al., 2010. Melting Relations of MORB-Sediment Melanges in Underplated Mantle Wedge Plumes; Implications for the Origin of Cordilleran-Type Batholiths. *Journal of Petrology*, 51(6): 1267–1295. https://doi.org/10.1093/petrology/egq019

Castro, A., Vogt, K., Gerya, T., 2013. Generation of New Continental Crust by Sublithospheric Silicic-Magma Relamination in Arcs: A Test of Taylor's Andesite Model. *Gondwana Research*, 23(4): 1554–1566. https://doi.org/10.1016/j.gr.2012.07.004

Chappell, B. W., 1996. Compositional Variation within Granite Suites of the Lachlan Fold Belt: Its Causes and Implications for the Physical State of Granite Magma. *Earth and Environmental Science Transactions of the Royal Society of Edinburgh*, 87(1/2): 159–170. https://doi.org/10.1017/s026359330000657x

Choudhary, A. K., Gopalan, K., Sastry, C. A., 1984. Present Status of the Geochronology of the Precambrian Rocks of Rajasthan. *Tectonophysics*, 105(1/2/3/4): 131–140. https://doi.org/10.1016/0040-1951(84)90199-9

Condie, K. C., Baragar, W. R. A., 1974. Rare-Earth Element Distributions in Volcanic Rocks from Archean Greenstone Belts. *Contributions to Mineralogy and Petrology*, 45(3): 237–246. https://doi.org/10.1007/bf00383441

Deb, M., Thorpe, R. I., Krstic, D., et al., 2001. Zircon U-Pb and Galena Pb Isotope Evidence for an Approximate 1.0 Ga Terrane Constituting the Western Margin of the Aravalli-Delhi Orogenic Belt, Northwestern India. *Precambrian Research*, 108(3/4): 195–213. https://doi.org/10.1016/s0301-9268(01)00134-6

Dhuime, B., Hawkesworth, C., Cawood, P., 2011. When Continents Formed. *Science*, 331(6014): 154–155. https://doi.org/10.1126/science.1201245

Eiler, J. M., 2001. Oxygen Isotope Variations of Basaltic Lavas and Upper Mantle Rocks. *Reviews in Mineralogy and Geochemistry*, 43(1): 319–364. https://doi.org/10.2138/gsrmg.43.1.319

Eiler, J. M., McInnes, B., Valley, J. W., et al., 1998. Oxygen Isotope Evidence for Slab-Derived Fluids in the Sub-Arc Mantle. *Nature*, 393(6687): 777–781. https://doi.org/10.1038/31679

Eiler, J. M., Schiano, P., Valley, J. W., et al., 2007. Oxygen-Isotope and Trace Element Constraints on the Origins of Silica-Rich Melts in the Subarc Mantle. *Geochemistry*, *Geophysics*, *Geosystems*, 8(9): Q09012. https://doi.org/10.1029/2006gc001503

Foley, S., Tiepolo, M., Vannucci, R., 2002. Growth of Early Continental Crust Controlled by Melting of Amphibolite in Subduction Zones. *Nature*, 417(6891): 837–840. https://doi.org/10.1038/nature00799

Gómez-Tuena, A., Mori, L., Rincón-Herrera, N. E., et al., 2008. The Origin of a Primitive Trondhjemite from the Trans-Mexican Volcanic Belt and Its Implications for the Construction of a Modern Continental Arc. *Geology*, 36(6): 471–474. https://doi.org/10.1130/g24687a.1

Griffin, W. L., Pearson, N. J., Belousova, E., et al., 2000. The Hf Isotope Composition of Cratonic Mantle: LAM-MC-ICPMS Analysis of Zircon Megacrysts in Kimberlites. *Geochimica et Cosmochimica Acta*, 64(1): 133–147. https://doi.org/10.1016/s0016-7037(99)00343-9

Griffin, W. L., Wang, X., Jackson, S. E., et al., 2002. Zircon Chemistry and Magma Mixing, SE China: *In-situ* Analysis of Hf Isotopes, Tonglu and Pingtan Igneous Complexes. *Lithos*, 61(3/4): 237–269. https://doi.org/10.1016/s0024-4937(02)00082-8

Hacker, B. R., Kelemen, P. B., Behn, M. D., 2011. Differentiation of the Continental Crust by Relamination. *Earth and Planetary Science Letters*, 307(3/4): 501–516. https://doi.org/10.1016/j.epsl.2011.05.024

Jagoutz, O., Schmidt, M. W., 2012. The Formation and Bulk Composition of Modern Juvenile Continental Crust: The Kohistan Arc. *Chemical Geology*, 298/299: 79–96. https://doi.org/10.1016/j.chemgeo.2011.10.022

Just, J., Schulz, B., de Wall, H., et al., 2011. Monazite CHIME/EPMA Dating of Erinpura Granitoid Deformation: Implications for Neoproterozoic Tectono-Thermal Evolution of NW India. *Gondwana Research*, 19(2): 402–412. https://doi.org/10.1016/j.gr.2010.08.002

Jweda, J., Bolge, L., Class, C., et al., 2015. High Precision Sr-Nd-Hf-Pb Isotopic Compositions of USGS Reference Material BCR-2. *Geostandards and Geoanalytical Research*, 40(1): 101–115. https://doi.org/10.1111/j.1751-908x.2015.00342.x

Kelemen, P. B., 1995. Genesis of High Mg# Andesites and the Continental Crust. *Contributions to Mineralogy and Petrology*, 120(1): 1–19. https://doi.org/10.1007/s004100050054

Kemp, A. I. S., Hawkesworth, C. J., Foster, G. L., et al., 2007. Magmatic and Crustal Differentiation History of Granitic Rocks from Hf-O Isotopes in Zircon. *Science*, 315(5814): 980–983. https://doi.org/10.1126/science.1136154

Klein, E. M., 2003. Geochemistry of the Igneous Oceanic Crust. In: Heinrich, D. H., Karl, K. T., eds., Treatise on Geochemistry. Pergamon, Oxford, 433–463. https://doi.org/10.1016/B0-08-043751-6/03030-9

Kröner, A., Windley, B. F., Badarch, G., et al., 2007. Accretionary Growth and Crust Formation in the Central Asian Orogenic Belt and Comparison with the Arabian-Nubian Shield. *Memoirs-Geological Society of America*, 200: 181. https://doi.org/10.1130/2007.1200(11)

Li, Q. L., Li, X. H., Liu, Y., et al., 2010. Precise U-Pb and Pb-Pb Dating of Phanerozoic Baddeleyite by SIMS with Oxygen Flooding Technique. *Journal of Analytical Atomic Spectrometry*, 25(7): 1107. https://doi.org/10.1039/b923444f

Liu, C. Z., Wu, F. Y., Chung, S. L., et al., 2014. A 'Hidden' ^{18}O-Enriched Reservoir in the Sub-Arc Mantle. *Scientific Reports*, 4(1): 4232. https://doi.org/10.1038/srep04232

Ludwig, K., 2003. User's Manual for Isoplot 3.00: A Geochronological Toolkit for Microsoft Excel. *Barkeley Geochronology Center Special Publication*, 4: 1–71

Lyu, P. L., Li, W. X., Wang, X.-C., et al., 2017. Initial Breakup of Supercontinent Rodinia as Recorded by ca. 860–840 Ma Bimodal Volcanism along the Southeastern Margin of the Yangtze Block, South China. *Precambrian Research*, 296: 148–167. https://doi.org/10.1016/j.precamres.2017.04.039

Martin, H., Smithies, R. H., Rapp, R., et al., 2005. An Overview of Adakite, Tonalite-Trondhjemite-Granodiorite (TTG), and Sanukitoid: Relationships and Some Implications for Crustal Evolution. *Lithos*, 79(1/2): 1–24. https://doi.org/10.1016/j.lithos.2004.04.048

Mattey, D., Lowry, D., Macpherson, C., 1994. Oxygen Isotope Composition of Mantle Peridotite. *Earth and Planetary Science Letters*, 128(3/4): 231–241. https://doi.org/10.1016/0012-821x(94)90147-3

Miller, J. A., Cartwright, I., Buick, I. S., et al., 2001. An O-Isotope Profile through the HP-LT Corsican Ophiolite, France and Its Implications for Fluid Flow during Subduction. *Chemical Geology*, 178(1/2/3/4): 43–69. https://doi.org/10.1016/s0009-2541(00)00428-9

Moyen, J. F., Martin, H., 2012. Forty Years of TTG Research. *Lithos*, 148: 312–336. https://doi.org/10.1016/j.lithos.2012.06.010

Naik, M. S., 1993. The Geochemistry and Genesis of the Granitoids of Sirohi, Rajasthan, India. *Journal of Southeast Asian Earth Sciences*, 8(1/2/3/4): 111–115. https://doi.org/10.1016/0743-9547(93)90012-e

Niu, Y. L., Zhao, Z. D., Zhu, D. C., et al., 2013. Continental Collision Zones are Primary Sites for Net Continental Crust Growth—A Testable Hypothesis.

Earth-Science Reviews, 127: 96–110. https://doi.org/10.1016/j.earscirev.2013.09.004

Pandit, M. K., Carter, L. M., Ashwal, L. D., et al., 2003. Age, Petrogenesis and Significance of 1 Ga Granitoids and Related Rocks from the Sendra Area, Aravalli Craton, NW India. *Journal of Asian Earth Sciences*, 22(4): 363–381. https://doi.org/10.1016/s1367-9120(03)00070-1

Pandit, M. K., Shekhawat, L. S., Ferreira, V. P., et al., 1999. Trondhjemite and Granodiorite Assemblages from West of Barmer: Probable Basement for Malani Magmatism in Western India. *Journal-Geological Society of India*, 53: 89–96. https://doi.org/10.1144/gsjgs.156.1.0191

Pradhan, V. R., Meert, J. G., Pandit, M. K., et al., 2010. India's Changing Place in Global Proterozoic Reconstructions: A Review of Geochronologic Constraints and Paleomagnetic Poles from the Dharwar, Bundelkhand and Marwar Cratons. *Journal of Geodynamics*, 50(3/4): 224–242. https://doi.org/10.1016/j.jog.2009.11.008

Rapp, R. P., Shimizu, N., Norman, M. D., 2003. Growth of Early Continental Crust by Partial Melting of Eclogite. *Nature*, 425(6958): 605–609. https://doi.org/10.1038/nature02031

Reagan, M. K., Hanan, B. B., Heizler, M. T., et al., 2008. Petrogenesis of Volcanic Rocks from Saipan and Rota, Mariana Islands, and Implications for the Evolution of Nascent Island Arcs. *Journal of Petrology*, 49(3): 441–464. https://doi.org/10.1093/petrology/egm087

Roy, A. B., Jakhar, S. R., 2002. Geology of Rajasthan (Northwest India)–Precambrian to Recent. Scientific Publishers (India), Jodhpur. xii+421

Smith, P. M., Asimow, P. D., 2005. Adiabat_1ph: A New Public Front-End to the MELTS, PMELTS, and PHMELTS Models. *Geochemistry*, *Geophysics*, *Geosystems*, 6(2): Q02004. https://doi.org/10.1029/2004gc000816

Solanki, A. M., 2011. A Petrographic, Geochemical, and Geochronological Investigation of Deformed Granitoids from SW Rajasthan: Neoproterozoic Age of Formation and Evidence of Pan-African Imprint: [Dissertation]. University of the Witwatersrand, Johannesburg. 216

Söderlund, U., Patchett, P. J., Vervoort, J. D., et al., 2004. The ^{176}Lu Decay Constant Determined by Lu-Hf and U-Pb Isotope Systematics of Precambrian Mafic Intrusions. *Earth and Planetary Science Letters*, 219(3/4): 311–324. https://doi.org/10.1016/s0012-821x(04)00012-3

Spandler, C., Pirard, C., 2013. Element Recycling from Subducting Slabs to Arc Crust: A Review. *Lithos*, 170/171: 208–223. https://doi.org/10.1016/j.lithos.2013.02.016

Sun, S. S., McDonough, W. F., 1989. Chemical and Isotopic Systematics of Oceanic Basalts: Implications for Mantle Composition and Processes. *Geological Society*, *London*, *Special Publications*, 42(1): 313–345. https://doi.org/10.1144/gsl.sp.1989.042.01.19

Valley, J. W., Bindeman, I. N., Peck, W. H., 2003. Empirical Calibration of Oxygen Isotope Fractionation in Zircon. *Geochimica et Cosmochimica Acta*, 67(17): 3257–3266. https://doi.org/10.1016/s0016-7037(03)00090-5

Valley, J. W., Kinny, P. D., Schulze, D. J., et al., 1998. Zircon Megacrysts from Kimberlite: Oxygen Isotope Variability among Mantle Melts. *Contributions to Mineralogy and Petrology*, 133(1/2): 1–11. https://doi.org/10.1007/s004100050432

Valley, J. W., Lackey, J. S., Cavosie, A. J., et al., 2005. 4.4 Billion Years of Crustal Maturation: Oxygen Isotope Ratios of Magmatic Zircon. *Contributions to Mineralogy and Petrology*, 150(6): 561–580. https://doi.org/10.1007/s00410-005-0025-8

Van Lente, B., Ashwal, L. D., Pandit, M. K., et al., 2009. Neoproterozoic Hydrothermally Altered Basaltic Rocks from Rajasthan, Northwest India: Implications for Late Precambrian Tectonic Evolution of the Aravalli Craton. *Precambrian Research*, 170(3/4): 202–222. https://doi.org/10.1016/j.precamres.2009.01.007

Vervoort, J. D., Plank, T., Prytulak, J., 2011. The Hf-Nd Isotopic Composition of Marine Sediments. *Geochimica et Cosmochimica Acta*, 75(20): 5903–5926. https://doi.org/10.1016/j.gca.2011.07.046

Volpe, A. M., Macdougall, J. D., 1990. Geochemistry and Isotopic Characteristics of Mafic (Phulad Ophiolite) and Related Rocks in the Delhi Supergroup, Rajasthan, India: Implications for Rifting in the Proterozoic. *Precambrian Research*, 48(1/2): 167–191. https://doi.org/10.1016/0301-9268(90)90061-t

Wang, X.-C., Li, Z.-X., Li, X.-H., et al., 2011. Nonglacial Origin for Low-^{18}O Neoproterozoic Magmas in the South China Block: Evidence from New *in-situ* Oxygen Isotope Analyses Using SIMS. *Geology*, 39(8): 735–738. https://doi.org/10.1130/g31991.1

Wang, X.-C., Wilde, S. A., Xu, B., et al., 2016. Origin of Arc-Like Continental Basalts: Implications for Deep-Earth Fluid Cycling and Tectonic Discrimination. *Lithos*, 261: 5–45. https://doi.org/10.1016/j.lithos.2015.12.014

White, L. T., Ireland, T. R., 2012. High-Uranium Matrix Effect in Zircon and Its Implications for SHRIMP U-Pb Age Determinations. *Chemical Geology*, 306/307: 78–91. https://doi.org/10.1016/j.chemgeo.2012.02.025

Wu, T., Zhou, J.-X., Wang, X.-C., et al., 2018. Identification of Ca. 850 Ma High-Temperature Strongly Peraluminous Granitoids in Southeastern Guizhou Province, South China: A Result of Early Extension along the Southern Margin of the Yangtze Block. *Precambrian Research*, 308: 18–34. https://doi.org/10.1016/j.precamres.2018.02.007

Yamaoka, K., Ishikawa, T., Matsubaya, O., et al., 2012. Boron and Oxygen Isotope Systematics for a Complete Section of Oceanic Crustal Rocks in the Oman Ophiolite. *Geochimica et Cosmochimica Acta*, 84: 543–559. https://doi.org/10.1016/j.gca.2012.01.043

Zhu, G. Z., Gerya, T. V., Tackley, P. J., et al., 2013. Four-Dimensional Numerical Modeling of Crustal Growth at Active Continental Margins. *Journal of Geophysical Research*: *Solid Earth*, 118(9): 4682–4698. https://doi.org/10.1002/jgrb.50357